

RESEARCH

Open Access



Multiple aromatic amino acids are involved in potyvirus movement by forming π -stackings to maintain coat protein accumulation

Zhi-Yong Yan¹, Xiao-Jie Xu¹, Le Fang¹, Chao Geng^{1,2}, Yan-Ping Tian^{1,2*} and Xiang-Dong Li^{1,2*} 

Abstract

Coat protein (CP) is required for potyviruses to move and establish a systemic infection in plants. π -stackings formed by aromatic residues play critical roles in maintaining protein stability and functions. As we know, many aromatic residues located in the core region of potyvirus CPs are conserved. However, their roles in potyvirus infection remain largely unknown. Here, through analysis of the three-dimensional model of the tobacco vein banding mosaic virus (TVBMV; genus *Potyvirus*) CP, 16 aromatic residues were predicated to form π -stackings. The results of transient expression experiments demonstrated that deletion of any of these 16 aromatic residues reduced CP accumulation. Infectivity assays showed that deletion of any of these aromatic residues in the TVBMV infectious clone abolished cell-to-cell movement and reduced replication of the virus. Substitution of Y¹⁰⁵ and Y¹⁴⁷ individually with non-aromatic residues alanine or glycine reduced CP accumulation, virus replication, and abolished the ability of TVBMV to move intercellularly, while substitution of these two residues individually with aromatic residues phenylalanine or tryptophan, had no or little effect on CP accumulation and TVBMV systemic movement and replication. Similar results were obtained from the CP mutants of watermelon mosaic virus (WMV, genus *Potyvirus*). Taken together, our results demonstrate that multiple aromatic residues in CP are involved in potyvirus movement by forming π -stackings to maintain CP accumulation.

Keywords: Coat protein, Movement, π -stacking, Potyvirus, Stability, Tobacco vein banding mosaic virus, Watermelon mosaic virus

Background

Potyviral CP is a multifunctional protein involved in encapsidation, aphid transmission, viral replication and movement (Weber and Bujarski 2015). It is divided into three regions: the N-terminal, the C-terminal and the conserved core regions (Shukla et al. 1988). The three-dimensional (3D) structures of CPs from three potyviruses, i.e., watermelon mosaic virus (WMV), potato virus Y (PVY) and turnip mosaic virus (TuMV), show

that the N- and C-terminal regions of CP are flexible and lack secondary structure, while the core region contains eight to ten α -helices and two β -sheet structures (Zamora et al. 2017; Cuesta et al. 2019; Kežar et al. 2019). The N- and C-terminal regions of CP are responsible for long-distance movement of tobacco etch virus (TEV) (Dolja et al. 1994, 1995). Maintaining the net charge of the N-terminal region is essential for cell-to-cell movement of zucchini yellow mosaic virus (ZYMV) (Kimalov et al. 2004). Substitutions of the charged residues in the C-terminal region of CP affect cell-to-cell movement of soybean mosaic virus (SMV) (Seo et al. 2013). Deletion of residues 6–50 in the CP N-terminus

* Correspondence: xdongli@sda.edu.cn; yanping.tian@sda.edu.cn

¹Laboratory of Plant Virology, College of Plant Protection, Shandong Agricultural University, Tai'an, Shandong 271018, People's Republic of China
Full list of author information is available at the end of the article



© The Author(s). 2021 **Open Access** This article is licensed under a Creative Commons Attribution 4.0 International License, which permits use, sharing, adaptation, distribution and reproduction in any medium or format, as long as you give appropriate credit to the original author(s) and the source, provide a link to the Creative Commons licence, and indicate if changes were made. The images or other third party material in this article are included in the article's Creative Commons licence, unless indicated otherwise in a credit line to the material. If material is not included in the article's Creative Commons licence and your intended use is not permitted by statutory regulation or exceeds the permitted use, you will need to obtain permission directly from the copyright holder. To view a copy of this licence, visit <http://creativecommons.org/licenses/by/4.0/>.

of TuMV has no obvious effect on its cell-to-cell and long-distance movement; while deletion of residues 265–274 in the CP C-terminus abolishes TuMV intercellular movement (Dai et al. 2020). Mutation of any of the conserved residues serine, arginine and aspartic acid at positions 122, 154 and 198, respectively (named as S¹²², R¹⁵⁴ and D¹⁹⁸) in the core region of CP abolishes cell-to-cell movement of TEV (Dolja et al. 1994, 1995). Mutations of residues corresponding to R¹⁵⁴ and D¹⁹⁸ of TEV CP in CPs of TuMV and wheat streak mosaic virus (WSMV, genus *Tritimovirus*, family *Potyviridae*) also abolish cell-to-cell movement of these two viruses (Tatineni et al. 2014; Dai et al. 2020). The residues at positions 192 and 225 (R¹⁹² and K²²⁵) located in the RNA binding pocket of CP are involved in cell-to-cell movement of TVBMV and WMV (Yan et al. 2021b). Recently, we have found that the conserved aromatic residue tryptophan at position 122 (W¹²²) in the core region of CP plays an important role in CP stability and cell-to-cell movement of TVBMV, PVY and WMV (Yan et al. 2021a).

Previous studies have shown that aromatic residues, including tyrosine (Y), phenylalanine (F) and tryptophan (W), are involved in protein stability and functions (Salonen et al. 2011; Chatterjee et al. 2019). The sidechains of aromatic residues in the core of a protein play essential roles in paired interactions (Burley and Petsko 1985). Mutation of the conserved aromatic residue F in the LFEYQ motif at the C-terminus of the readthrough protein of potato leafroll virus reduces long-distance movement of the virus and symptom expression (Xu et al. 2018). Changing the aromatic residue Y³⁹⁸ in the nonstructural protein S (NSs) of watermelon silver mottle virus reduces the strength of self-interaction and stability of the protein, and also virus pathogenicity on squash plants (Huang et al. 2015). Two rings of aromatic residues with a centroid distance less than 10.0 Å can form π -stacking (Burley and Petsko 1985). π -stacking is involved in recognizing the mRNA cap-binding protein (eukaryotic initiation factor 4E) (Marcotrigiano et al. 1997; Matsuo et al. 1997). π -stacking plays essential roles in maintaining the stability of several proteins, including small ribonuclease barnase in *Bacillus amyloliquefaciens*, the outer membrane protein and the cold shock protein in *Escherichia coli* (Serrano et al. 1991; Hillier et al. 1998; Hong et al. 2007). The aromatic residue pair Y⁵¹-F⁶⁴ in small ubiquitin-like modifier (SUMO) protein forms a specific edge-to-face conformation, which is vital for SUMO fold and stability (Chatterjee et al. 2019). The carp parvalbumin protein contains a cluster of seven F residues that can form a stereotypic aromatic ring network,

which is essential for maintaining functional structure (Burley and Petsko 1985). To date, little is known about the function of π -stackings in regulating virus infection.

Here, we found that multiple conserved aromatic residues in the CPs of TVBMV and WMV could form π -stackings, which are essential for maintaining CP accumulation and virus movement. Our finding provides new insight into the role of evolutionarily conserved aromatic residues of CP in potyvirus infection.

Results

Sixteen aromatic residues in TVBMV CP are predicted to form π -stackings

It has been demonstrated that the π -stacking structure can be formed with a centroid distance less than 10.0 Å between two rings of aromatic residues (Burley and Petsko 1985). Here, sequence analysis showed there were 18 aromatic residues in TVBMV CP in addition to the previously reported W¹²² (Yan et al. 2021a). All the 19 aromatic residues were located in the core region of CP. To determine whether these aromatic residues could form π -stacking, we measured the centroid distance between aromatic residue rings based on the predicted 3D model of TVBMV CP. The results showed that residues F⁴⁶, Y⁷⁷ or F²³⁷ could not form π -stacking with any other aromatic residues within TVBMV CP, but other 16 aromatic residues, including F⁹⁴, W⁹⁷, Y⁹⁸, Y¹⁰⁵, W¹²², W¹³⁶, Y¹⁴⁷, F¹⁶⁰, F¹⁶⁷, Y¹⁷⁴, Y¹⁸⁴, Y¹⁸⁸, Y²⁰², F²⁰⁴, F²⁰⁶ and Y²⁰⁷, could form π -stackings (Fig. 1 and Additional file 1: Table S1). Residues Y¹⁰⁵ and W¹²² could form one π -stacking with Y¹⁴⁷ and W¹³⁶, respectively; residues Y⁹⁸, Y¹⁴⁷ and Y¹⁸⁴ could form two π -stackings with other aromatic residues; residues F⁹⁴, W¹³⁶, Y¹⁷⁴ and Y²⁰² could form three π -stackings with other aromatic residues; residues W⁹⁷, F¹⁶⁰, F¹⁶⁷, Y¹⁸⁸ and Y²⁰⁷ could form four π -stackings with other aromatic residues; residues F²⁰⁴ and F²⁰⁶ could form six π -stackings with other aromatic residues (Fig. 1 and Additional file 1: Table S1).

The π -stackings are essential for maintaining CP accumulation

To determine the role of π -stackings in TVBMV CP accumulation, we individually deleted each of the above-mentioned 16 aromatic residues that could form π -stacking in the transient expression construct pCamGFP-TVBMVCP (the expressed protein was named as GFP-TVBMVCP) to produce their corresponding mutant plasmids, including pCamGFP-TVBMVCP (Δ F94), pCamGFP-TVBMVCP (Δ W97), pCamGFP-TVBMVCP (Δ Y98), pCamGFP-TVBMVCP (Δ Y105), pCamGFP-TVBMVCP (Δ W122), pCamGFP-

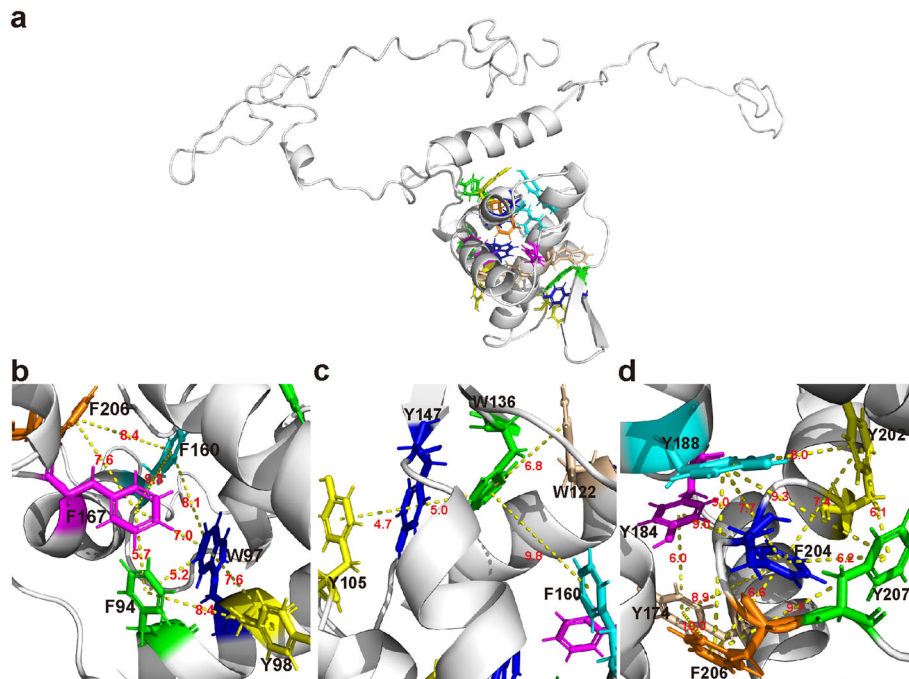


Fig. 1 π -stacking analysis based on the predicted TVBMV CP 3D model. **a** The overview of the predicted TVBMV CP 3D cartoon model. Sixteen aromatic residues forming π -stackings are indicated in sticks. **b–d** The close view of the π -stackings between 16 aromatic residues in TVBMV CP. The positions of F⁹⁴, W⁹⁷, Y⁹⁸, F¹⁶⁰, F¹⁶⁷ and F²⁰⁶ indicated with different colors are shown in **b**. The positions of Y¹⁰⁵, W¹²², W¹³⁶, Y¹⁴⁷ and F¹⁶⁰ indicated with different colors are shown in **c**. The positions of Y¹⁷⁴, Y¹⁸⁴, Y¹⁸⁸, Y²⁰², F²⁰⁴, F²⁰⁶ and Y²⁰⁷ indicated with different colors are shown in **d**. The centroid distance less than 10 Å between two aromatic rings is indicated with a yellow dash line and the corresponding distance values are indicated with red fonts

TVBMVCP (Δ W136), pCamGFP-TVBMVCP (Δ Y147), pCamGFP-TVBMVCP (Δ F160), pCamGFP-TVBMVCP (Δ F167), pCamGFP-TVBMVCP (Δ Y174), pCamGFP-TVBMVCP (Δ Y184), pCamGFP-TVBMVCP (Δ Y188), pCamGFP-TVBMVCP (Δ Y202), pCamGFP-TVBMVCP (Δ F204), pCamGFP-TVBMVCP (Δ F206) and pCamGFP-TVBMVCP (Δ Y207). Meanwhile, deletions were also introduced into codons coding for F⁴⁶, Y⁷⁷ and F²³⁷ that could not form π -stacking, and the resultant mutants were named pCamGFP-TVBMVCP (Δ F46), pCamGFP-TVBMVCP (Δ Y77) and pCamGFP-TVBMVCP (Δ F237), respectively. *Agrobacterium* ($OD_{600} = 0.4$) carrying plasmid pCamGFP-TVBMVCP or one of the 19 mutant plasmids was infiltrated into fully expanded leaves of *N. benthamiana*. At 5 days post-agro-infiltration (dpai), the expression level of GFP-TVBMVCP (Δ F46) was similar to that of GFP-TVBMVCP, and those of GFP-TVBMVCP (Δ Y77) and GFP-TVBMVCP (Δ F237) were reduced to 60 and 80% of that of GFP-TVBMVCP, respectively, while those of the rest 16 mutant proteins were less than 20% of that of GFP-TVBMVCP (Fig. 2a, b). These results indicate that π -stackings are essential for maintaining TVBMV CP accumulation.

The π -stackings are required for cell-to-cell movement and replication of TVBMV

To determine the role of π -stackings in TVBMV infection of *N. benthamiana* plants, we individually introduced each deleted mutation of aromatic residues that could form π -stacking into a GFP-expressing TVBMV infectious clone pCamTVBMV-GFP (the produced virus was named as TVBMV-GFP) to produce mutant plasmids, including pCamTVBMV-GFP (Δ F94), pCamTVBMV-GFP (Δ W97), pCamTVBMV-GFP (Δ Y98), pCamTVBMV-GFP (Δ Y105), pCamTVBMV-GFP (Δ W122), pCamTVBMV-GFP (Δ W136), pCamTVBMV-GFP (Δ Y147), pCamTVBMV-GFP (Δ F160), pCamTVBMV-GFP (Δ F167), pCamTVBMV-GFP (Δ Y174), pCamTVBMV-GFP (Δ Y184), pCamTVBMV-GFP (Δ Y188), pCamTVBMV-GFP (Δ Y202), pCamTVBMV-GFP (Δ F204), pCamTVBMV-GFP (Δ F206) and pCamTVBMV-GFP (Δ Y207). We also deleted the codon coding for F⁴⁶, which could not form π -stacking with other aromatic residues within CP, in the pCamTVBMV-GFP to produce pCamTVBMV-GFP (Δ F46) and used it as a control. *Agrobacterium* ($OD_{600} = 0.2$) carrying pCamTVBMV-GFP or one of the mutant plasmids was infiltrated

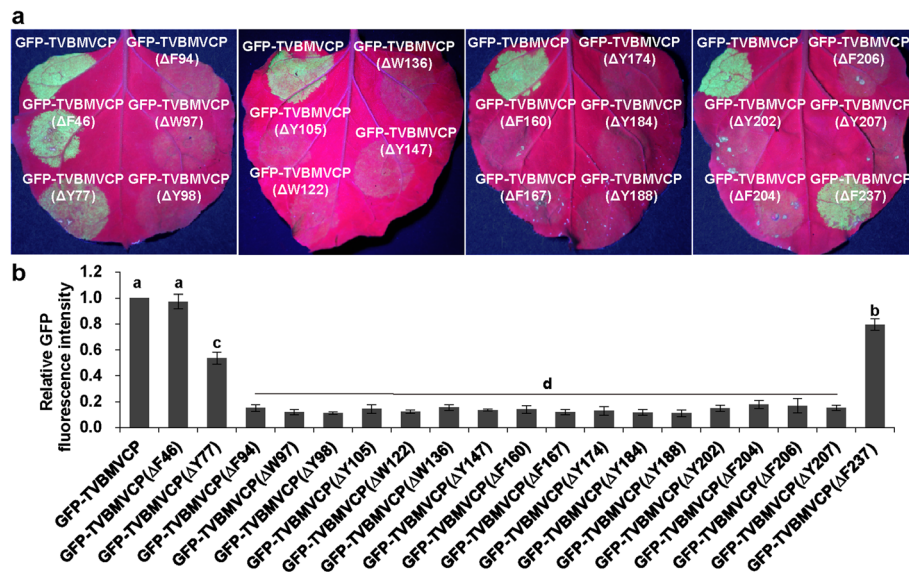


Fig. 2 Effect of π -stackings on CP accumulation. **a** GFP fluorescence and **b** relative GFP fluorescence intensities in the *N. benthamiana* leaf patches expressing GFP-TVBMVCP, one of its 16 mutants derived from aromatic residues (F⁹⁴, W⁹⁷, Y⁹⁸, Y¹⁰⁵, W¹²², W¹³⁶, Y¹⁴⁷, F¹⁶⁰, F¹⁶⁷, Y¹⁷⁴, Y¹⁸⁴, Y¹⁸⁸, Y²⁰², F²⁰⁴, F²⁰⁶ and Y²⁰⁷) that were predicted to form π -stacking, or one of its 3 mutants derived from aromatic residues (F⁴⁶, Y⁷⁷ and F²³⁷) that could not form π -stacking at 5 dpi. 'Δ' indicates the codon for the residue was deleted. The values are the means \pm SD from three biological replicates per treatment. Treatments marked with the same lowercase letters have no significant statistical difference

into leaves of *N. benthamiana* plants. At 7 dpi, GFP fluorescence was observed not only in the infiltrated leaves but also in the systemic leaves of *N. benthamiana* plants when agrobacterium carrying TVBMV-GFP or TVBMV-GFP (Δ F46). However, GFP fluorescence was observed only in the infiltrated leaves of *N. benthamiana* plants when agrobacterium carrying each of the 16 mutants, as illustrated by TVBMV-GFP (Δ Y105) and TVBMV-GFP (Δ Y147) (Fig. 3a). Enzyme-linked immunosorbent assay (ELISA) results also showed that the virus was detected in the systemic leaves of plants when agrobacterium carrying TVBMV-GFP or TVBMV-GFP (Δ F46), rather than other mutant viruses was infiltrated (Fig. 3b).

To examine cell-to-cell movement of these systemic movement-defective mutants, we infiltrated the agrobacterium ($OD_{600} = 0.0001$) carrying one of these 16 mutant plasmids into *N. benthamiana* leaves. At 5 dpi, the leaves inoculated were observed under a confocal microscope. We analyzed 30 fluorescent foci for each mutant. The results showed that GFP fluorescence produced by the 16 mutant viruses was confined only to single cells (Fig. 3c), as illustrated by TVBMV-GFP (Δ Y105) and TVBMV-GFP (Δ Y147), whereas the fluorescence signal produced by TVBMV-GFP was observed to spread to many neighboring cells (Fig. 3d).

We further determined the viral RNA accumulation levels of these 16 mutant viruses. Agrobacterium ($OD_{600} = 0.2$) carrying pCamTVBMV-GFP or one of the

16 mutant plasmids was infiltrated into *N. benthamiana* leaves. The replication-defective mutants pCamTVBMV-GFP (Nib Δ GDD) and pCamTVBMV-GFP (CPSTOP), in which the codon encoding residues GDD in Nib was deleted, or a stop codon was inserted between the first and second codon of CP-encoding sequence in pCamTVBMV-GFP, were used as controls (Geng et al. 2017; Yan et al. 2021a). At 60 h post-agro-infiltration (hpai), the viral minus (-)RNA accumulating levels were detected by using reverse transcription-quantitative polymerase chain reaction (RT-qPCR). It was showed that viral (-)RNA accumulating levels of these 16 mutants amounted to 30–40% of that of TVBMV-GFP, while those of TVBMV-GFP (Nib Δ GDD) and TVBMV-GFP (CPSTOP) were \sim 20% of that of TVBMV-GFP (Fig. 3e). There was no significant difference in (-)RNA accumulating level among mutant viruses derived from these 16 aromatic residues (Fig. 3e). These results indicate that π -stackings are critical for cell-to-cell movement and replication of TVBMV.

Mutations retaining π -stackings can maintain CP accumulation, replication and movement of TVBMV

To test whether the mutations retaining π -stackings could maintain TVBMV CP accumulation, we selected two aromatic residues Y¹⁰⁵ and Y¹⁴⁷, which could form π -stacking, for non-aromatic or aromatic substitution experiments. We individually substituted the codon for Y¹⁰⁵ or Y¹⁴⁷ in pCamGFP-TVBMVCP with that for non-

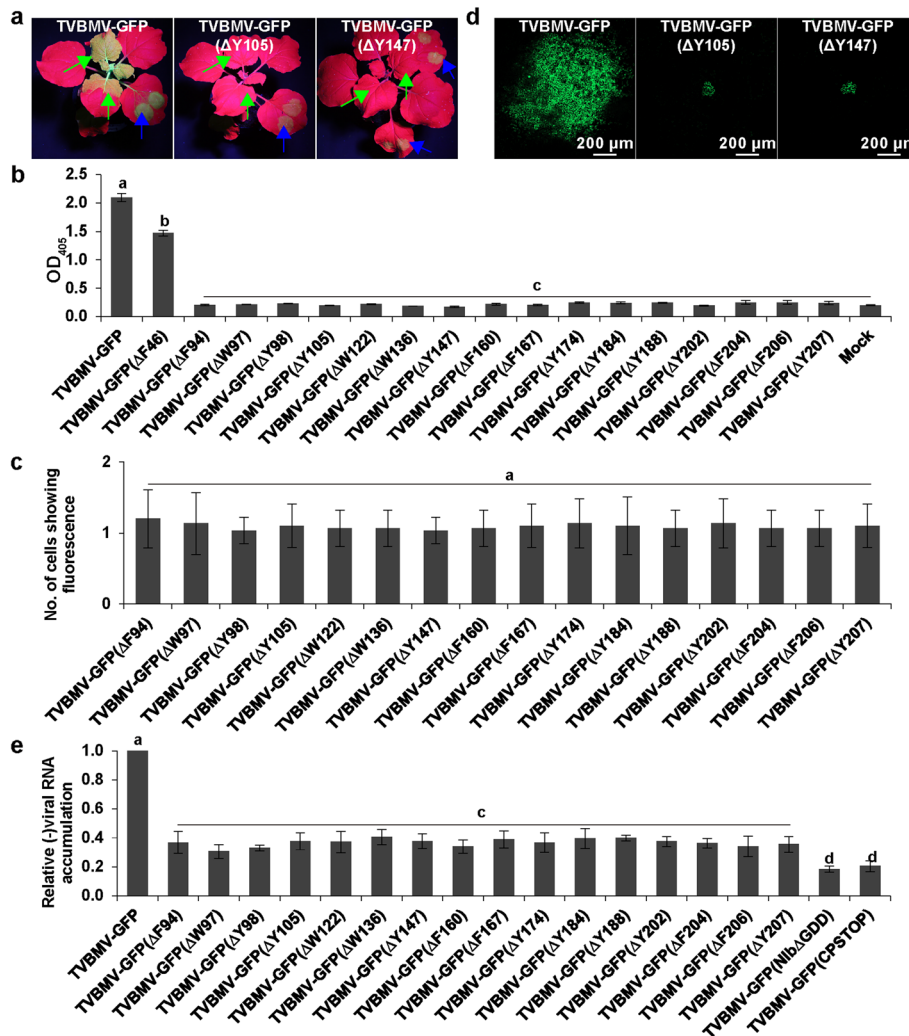


Fig. 3 Effect of π -stackings on systemic and cell-to-cell movement, and replication of TVBMV. **a** Systemic movement of TVBMV-GFP, TVBMV-GFP (Δ Y105) and TVBMV-GFP (Δ Y147). GFP fluorescence in the systemic leaves of *N. benthamiana* plants inoculated with the virus was observed under UV light at 7 dpai. Blue and green arrows indicate the infiltrated and systemic leaves, respectively. **b** Viral accumulation was detected by ELISA in the systemic leaves of *N. benthamiana* plants inoculated with TVBMV-GFP, one of its 16 mutants derived from aromatic residues (F⁹⁴, W⁹⁷, Y⁹⁸, Y¹⁰⁵, W¹²², W¹³⁶, Y¹⁴⁷, F¹⁶⁰, F¹⁶⁷, Y¹⁷⁴, Y¹⁸⁴, Y¹⁸⁸, Y²⁰², F²⁰⁴, F²⁰⁶ and Y²⁰⁷) that were predicted to form π -stacking, or TVBMV-GFP (Δ F46) at 7 dpai. A sample from a buffer-inoculated plant was used as a negative control (Mock). **c** Cell-to-cell movement of 16 viral mutants in the infiltrated leaves at 5 dpai. The number of cells showing GFP fluorescence was the means \pm SD from 30 infection foci per treatment. **d** Cell-to-cell movement of TVBMV-GFP, TVBMV-GFP (Δ Y105), and TVBMV-GFP (Δ Y147). GFP fluorescence was observed under a confocal microscope at 5 dpai. **e** The replication levels of TVBMV-GFP, viral mutants derived from 16 aromatic residues, and replication-defective mutants TVBMV-GFP (Nib Δ GDD) and TVBMV-GFP (CPSTOP). The minus-strand (-)RNA accumulating level in the infiltrated leaf patches was detected by RT-qPCR at 60 hpai. The expression level of *NbEF1A* was used as an internal control. The values are the means \pm SD from three biological replicates per treatment. Treatments marked with the same lowercase letters have no significant statistical difference. The inoculation tests were repeated three times independently. The viral systemic and cell-to-cell movement in the plants inoculated with the other 14 aromatic mutants were the same as those in the plants inoculated with TVBMV-GFP (Δ Y105) and TVBMV-GFP (Δ Y147) (data are not shown). ‘ Δ ’ indicates the codon for the residue has been deleted

aromatic residues A and G, or aromatic residues F and W to produce pCamGFP-TVBMVCP(Y105A), pCamGFP-TVBMVCP(Y105G), pCamGFP-TVBMVCP(Y147A), pCamGFP-TVBMVCP(Y147G), pCamGFP-TVBMVCP(Y105F), pCamGFP-TVBMVCP(Y105W), pCamGFP-TVBMVCP(Y147F) and pCamGFP-TVBMVCP(Y147W).

N. benthamiana leaves were infiltrated with agrobacterium (OD₆₀₀ = 0.4) harboring pCamGFP-TVBMVCP or one of the above eight mutant plasmids. At 5 dpai, the GFP fluorescence intensity in the patches expressing GFP-TVBMVCP(Y105A), GFP-TVBMVCP(Y105G), GFP-TVBMVCP(Y147A) or GFP-TVBMVCP(Y147G) was

similar to that expressing GFP-TVBMVCP ($\Delta Y105$) or GFP-TVBMVCP ($\Delta Y147$), less than 20% of that of GFP-TVBMVCP. In contrast, GFP fluorescence intensity in the patches expressing GFP-TVBMVCP(Y105F), GFP-TVBMVCP(Y147F) or GFP-TVBMVCP(Y147W) was similar to that expressing GFP-TVBMVCP. We also noted that GFP fluorescence intensity produced by GFP-TVBMVCP(Y105W) was approximately 75% of that by GFP-TVBMVCP (Fig. 4a, b). To exclude the effect of GFP on CP accumulation, we substituted the codon for Y¹⁰⁵ or Y¹⁴⁷ to that for A and G in pCamTVBMVCP, which could express TVBMV CP, to produce pCamTVBMVCP(Y105A), pCamTVBMVCP(Y105G), pCamTVBMVCP(Y147A) and pCamTVBMVCP(Y147G). The CP accumulation was detected by western blotting at 5 dpai. The results showed that the CP accumulation levels of these four mutants was significantly lower than that of TVBMVCP (Additional file 2: Figure S1). These results indicate that π -stacking formed by Y¹⁰⁵ and Y¹⁴⁷ is critical for TVBMV CP accumulation.

To determine whether the mutations retaining π -stackings can maintain TVBMV systemic movement, we individually introduced mutations of Y105A, Y105G, Y147A, Y147G, Y105F, Y105W, Y147F and Y147W into pCamTVBMV-GFP to produce pCamTVBMV-GFP(Y105A), pCamTVBMV-GFP(Y105G), pCamTVBMV-GFP(Y147A), pCamTVBMV-GFP(Y147G), pCamTVBMV-GFP(Y105F), pCamTVBMV-GFP(Y105W), pCamTVBMV-GFP(Y147F) and pCamTVBMV-GFP(Y147W), respectively. *Agrobacterium* (OD₆₀₀ = 0.2) harboring pCamTVBMV-GFP or one of these eight mutant plasmids was infiltrated into *N. benthamiana* plants. At 7 dpai, TVBMV-GFP, TVBMV-GFP(Y105F), TVBMV-GFP(Y105W), TVBMV-GFP(Y147F) and TVBMV-GFP(Y147W) could, whereas TVBMV-GFP(Y105A), TVBMV-GFP(Y105G), TVBMV-GFP(Y147A) and TVBMV-GFP(Y147G) could not move systemically in *N. benthamiana* plants (Fig. 4c). The RT-qPCR results showed that no viral RNA of TVBMV-GFP(Y105A), TVBMV-GFP(Y105G), TVBMV-GFP(Y147A) and TVBMV-GFP(Y147G) was detected in the systemic leaves of the assayed plants. TVBMV-GFP(Y105F) and TVBMV-GFP(Y147F) accumulated to a similar level of viral RNA compared with TVBMV-GFP. TVBMV-GFP(Y105W) and TVBMV-GFP(Y147W) accumulated to ~ 50% level of viral RNA of TVBMV-GFP (Fig. 4d).

To further confirm the role of π -stacking formed by Y¹⁰⁵ and Y¹⁴⁷ in viral cell-to-cell movement, we infiltrated the *Agrobacterium* (OD₆₀₀ = 0.0001) carrying pCamTVBMV-GFP or one of the eight mutant plasmids into *N. benthamiana* leaves. At 5 dpai, TVBMV-GFP, TVBMV-GFP(Y105F), TVBMV-GFP(Y105W), TVBMV-GFP(Y147F) and TVBMV-GFP(Y147W) were observed to spread to many cells, but TVBMV-GFP(Y105A),

TVBMV-GFP(Y105G), TVBMV-GFP(Y147A) and TVBMV-GFP(Y147G) could not move intercellularly (Fig. 4e–g).

We further detected the viral RNA accumulation in the infiltrated leaves at 60 hpai. RT-qPCR results showed that the (–)RNA accumulation levels of TVBMV-GFP(Y105A), TVBMV-GFP(Y105G), TVBMV-GFP(Y147A) and TVBMV-GFP(Y147G) were approximately 40% of that of TVBMV-GFP (Fig. 4h). The (–)RNA accumulation levels of TVBMV-GFP(Y105F), TVBMV-GFP(Y147F) and TVBMV-GFP(Y147W) were similar to that of TVBMV-GFP, and it was 80% of that of TVBMV-GFP for TVBMV-GFP(Y105W) (Fig. 4h).

These results indicate that mutations retaining π -stackings can maintain CP accumulation, replication and movement of TVBMV.

Disrupting π -stackings reduces virus particle number

To determine the effect of π -stackings on virus particle assembly and yield, we purified virus particles from the agroinfiltrated leaves. The extracts were negatively stained and then observed under transmission electron microscopy. The results showed that typical virus particles were easily observed in leaf samples treated with TVBMV-GFP, TVBMV-GFP(Y105F), TVBMV-GFP(Y105W), TVBMV-GFP(Y147F) and TVBMV-GFP(Y147W). However, virus particles in leaf samples treated with TVBMV-GFP(Y105A), TVBMV-GFP(Y105G), TVBMV-GFP(Y147A) and TVBMV-GFP(Y147G) were barely detected (Fig. 5a, b). These results indicate that destroying the π -stackings does not completely abolish the ability of mutant viruses to assemble virus particles, but significantly reduces the number of virus particles.

The π -stackings play essential roles in CP accumulation and cell-to-cell movement of WMV

Sequence analysis of 234 potyvirus CP sequences showed that among the 16 aromatic residues in TVBMV CP that could form π -stackings, 11 residues were completely conserved, and the rest five were incompletely conserved (Additional file 2: Figure S2), indicating that π -stackings were conserved in potyvirus CPs.

We compared the predicted 3D model of TVBMV CP with those of PVY, WMV and TuMV CPs (Zamora et al. 2017; Cuesta et al. 2019; Kežar et al. 2019), and found that they shared structural similarities (Additional file 2: Figure S3). The same as in TVBMV CP, there were 19 aromatic residues in WMV CP, and all of them were located in the core region of WMV CP. Sixteen of them, including F¹⁰⁵, W¹⁰⁸, Y¹⁰⁹, Y¹¹⁶, F¹³⁰, W¹³³, W¹⁴⁷, Y¹⁵⁸, F¹⁷⁸, Y¹⁸⁵, Y¹⁹⁵, Y¹⁹⁹, Y²¹³, F²¹⁵, F²¹⁷ and Y²¹⁸, were predicted to form π -stackings, whereas the rest three aromatic residues, including Y⁸⁸, F⁹⁶ and F²⁴⁸, could not form this structure (Fig. 6 and Additional file 1: Table S2). Sequence analysis

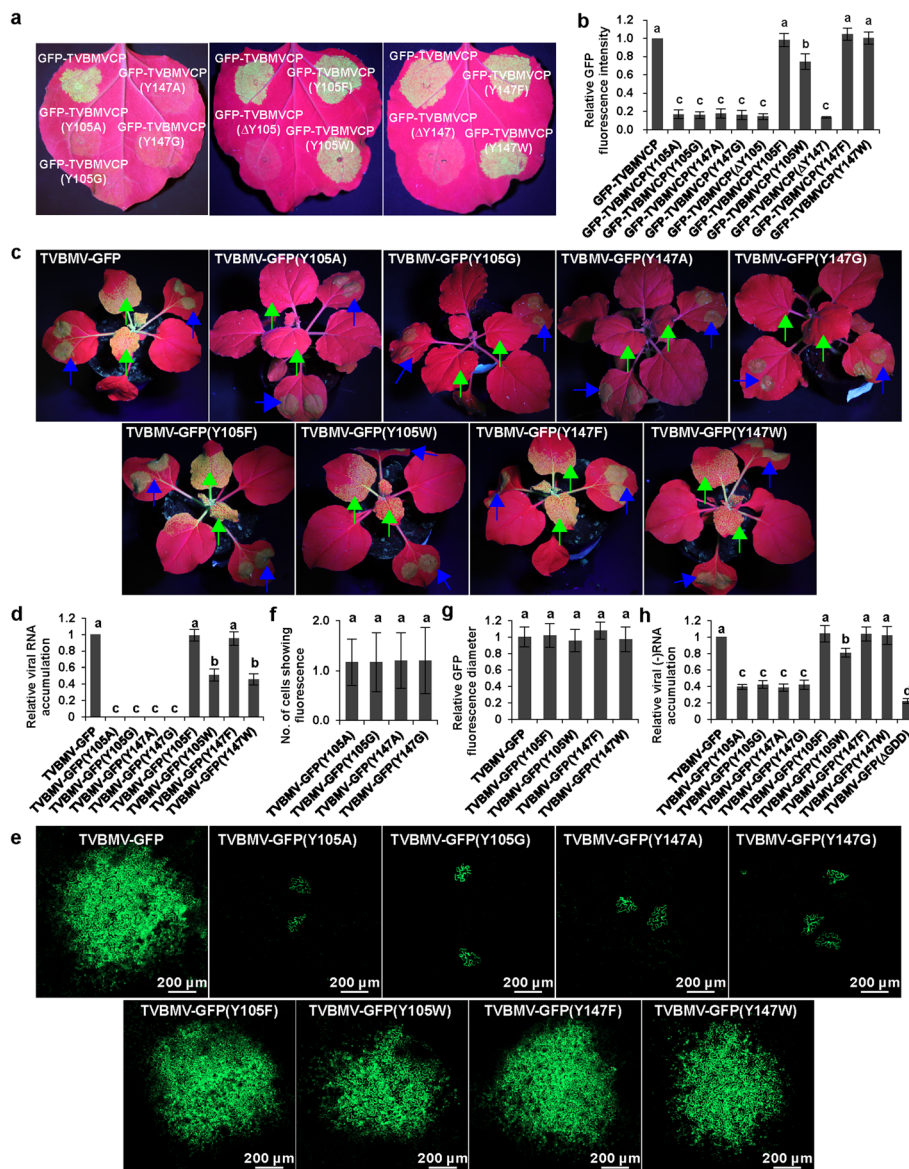


Fig. 4 Effects of substitution retaining π -stackings on CP accumulation, replication and movement of TVBMV. **a** GFP fluorescence and **b** relative GFP fluorescence intensities in the *N. benthamiana* leaf patches expressing GFP-TVBMVCP, GFP-TVBMV(Y105A), GFP-TVBMV(Y105G), GFP-TVBMV(Y147A), GFP-TVBMV(Y147G), GFP-TVBMVCP (Δ Y105), GFP-TVBMVCP(Y105F), GFP-TVBMVCP(Y105W), GFP-TVBMVCP (Δ Y147), GFP-TVBMVCP(Y147F) and GFP-TVBMVCP(Y147W) at 5 dpi. Pictures were photographed under UV light. GFP fluorescence intensities were determined by a multi-function microplate reader. ' Δ ' indicates the codon for the residue has been deleted. **c** GFP fluorescence and **d** viral RNA accumulation level in the systemic leaves of *N. benthamiana* inoculated with TVBMV-GFP, TVBMV-GFP(Y105A), TVBMV-GFP(Y105G), TVBMV-GFP(Y147A), TVBMV-GFP(Y147G), TVBMV-GFP(Y105F), TVBMV-GFP(Y105W), TVBMV-GFP(Y147F) and TVBMV-GFP(Y147W) at 7 dpi. Viral RNA accumulation was determined by RT-qPCR. Blue and green arrows indicate the infiltrated and systemic leaves, respectively. **e** Cell-to-cell movement of TVBMV-GFP, TVBMV-GFP(Y105A), TVBMV-GFP(Y105G), TVBMV-GFP(Y147A), TVBMV-GFP(Y147G), TVBMV-GFP(Y105F), TVBMV-GFP(Y105W), TVBMV-GFP(Y147F) and TVBMV-GFP(Y147W). GFP fluorescence was observed under a confocal microscope at 5 dpi. **f** The number of cells showing GFP fluorescence in each infection locus of TVBMV-GFP(Y105A), TVBMV-GFP(Y105G), TVBMV-GFP(Y147A) and TVBMV-GFP(Y147G). **g** The diameter of cells showing GFP fluorescence in each infection locus of TVBMV-GFP, TVBMV-GFP(Y105F), TVBMV-GFP(Y105W), TVBMV-GFP(Y147F) and TVBMV-GFP(Y147W). The values are the means \pm SD from 30 infection foci per treatment. **h** The minus-strand (-) RNA accumulating level in the infiltrated leaf patches of *N. benthamiana* inoculated with TVBMV-GFP, TVBMV-GFP(Y105A), TVBMV-GFP(Y105G), TVBMV-GFP(Y147A), TVBMV-GFP(Y147G), TVBMV-GFP(Y105F), TVBMV-GFP(Y105W), TVBMV-GFP(Y147F), TVBMV-GFP(Y147W) or replication-defective mutant TVBMV-GFP (Nib Δ GDD) detected by RT-qPCR at 60 hpi, with the expression of *NbEF1A* as an internal control. The values are the means \pm SD from three biological replicates per treatment. Treatments marked with the same lowercase letters have no significant statistical difference

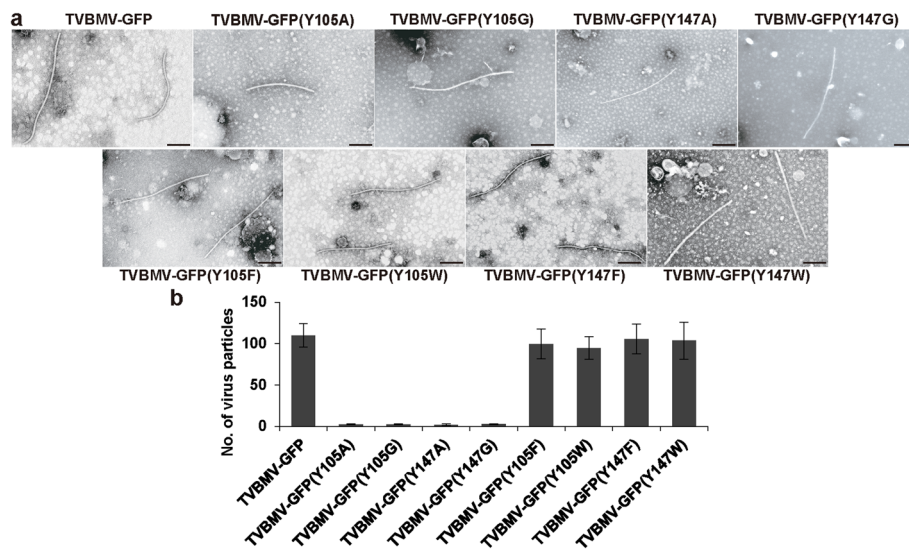


Fig. 5 Effect of π -stackings on virus particle assembly. **a** Virion of TVBMV-GFP or its mutants. Scale bar = 200 nm. The virus particles were purified from the infiltrated leaf tissues at 6 dpi. **b** The number of virus particles. Virus particles were counted in a field of 225 μm^2 for each treatment. The values are the means \pm SD from three fields per treatment

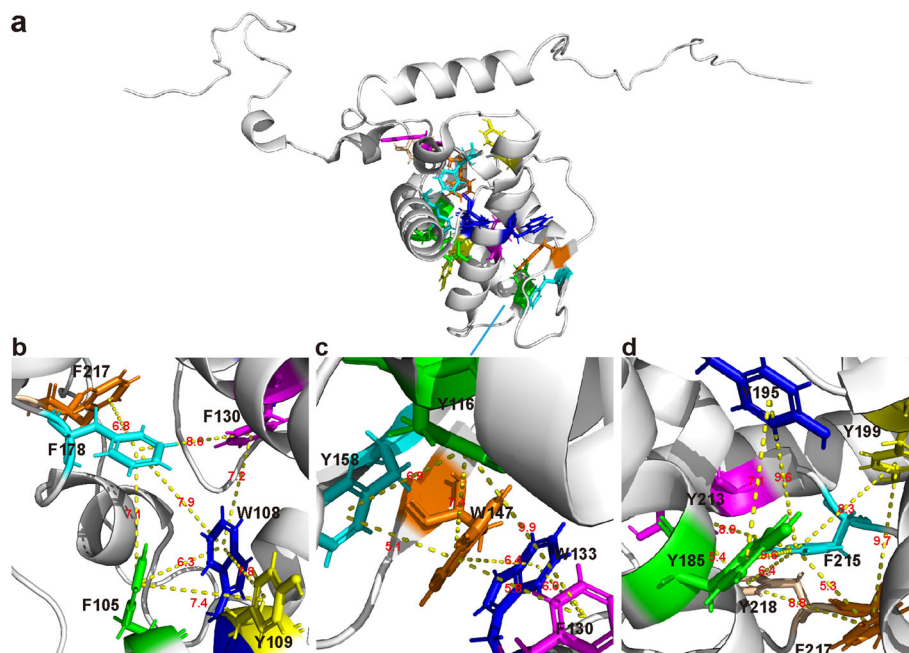


Fig. 6 π -stackings analysis based on the WMV CP 3D structure. **a** The overview of WMV CP 3D cartoon structure. Sixteen aromatic residues forming π -stackings are shown in sticks. **b–d** The close views of the π -stackings between 16 aromatic residues in WMV CP. The positions of F¹⁰⁵, W¹⁰⁸, Y¹⁰⁹, F¹³⁰, F¹⁷⁸ and F²¹⁷ indicated with different colors are shown in **b**. The positions of Y¹¹⁶, F¹³⁰, W¹³³, W¹⁴⁷ and Y¹⁵⁸ indicated with different colors are shown in **c**. The positions of Y¹⁸⁵, Y¹⁹⁵, Y¹⁹⁹, Y²¹³, F²¹⁵, F²¹⁷ and Y²¹⁸ indicated with different colors are shown in **d**. The centroid distance less than 10 Å between two aromatic rings is indicated with a yellow dash line and the corresponding distance values are indicated with red fonts

showed that 15 of these 16 aromatic residues in WMV CP were identical to that in the corresponding positions in TVBMV CP (Additional file 2: Figure S4).

We individually deleted the codon for these 19 aromatic residues from pCamGFP-WMVCP that express GFP-WMVCP, a fusion protein of GFP and wild-type WMV CP, to produce 19 mutant plasmids. The *N. benthamiana* leaves were infiltrated with agrobacterium carrying pCamGFP-WMVCP or one of these 19 mutants. At 5 dpai, GFP fluorescence intensity in the leaf patches expressing one of 16 mutants decreased to 20–40% of that of GFP-WMVCP, and it was 60% of that of GFP-WMVCP for GFP-WMVCP (ΔF96). For GFP-WMVCP (ΔY88) and GFP-WMVCP (ΔF248), the same level of fluorescence intensities with that of GFP-WMVCP were observed (Fig. 7a, b). These results indicate that mutations disrupting any π -stackings compromise the accumulation of WMV CP.

To investigate the effects of π -stacking on WMV movement, we individually deleted the codons for the 16 aromatic residues that could form π -stackings from the WMV infectious clone pCBWMV-GFP (WMV-GFP) to produce the corresponding virus mutants. *N. benthamiana* leaves were infiltrated with agrobacterium (OD₆₀₀ = 0.0001) harboring pCBWMV-GFP or one of these 16 mutant plasmids. At 5 dpai, WMV-GFP was found to have spread to many cells in the infiltrated leaf patches. In contrast, GFP fluorescence in the WMV-GFP (ΔF105)-, WMV-GFP (ΔW108)-, WMV-GFP (ΔY109)-, WMV-GFP (ΔY116)-, WMV-GFP (ΔF130)-, WMV-GFP (ΔW133)-, WMV-GFP (ΔW147)-, WMV-GFP (ΔY158)-, WMV-GFP (ΔF178)-, WMV-GFP (ΔY185)-, WMV-GFP (ΔY195)-, WMV-GFP (ΔY199)-, WMV-GFP (ΔY213)-, WMV-GFP (ΔF215)-, WMV-GFP (ΔF217)- and WMV-GFP (ΔY218)-inoculated leaf patches was only confined to single cells (Fig. 7c).

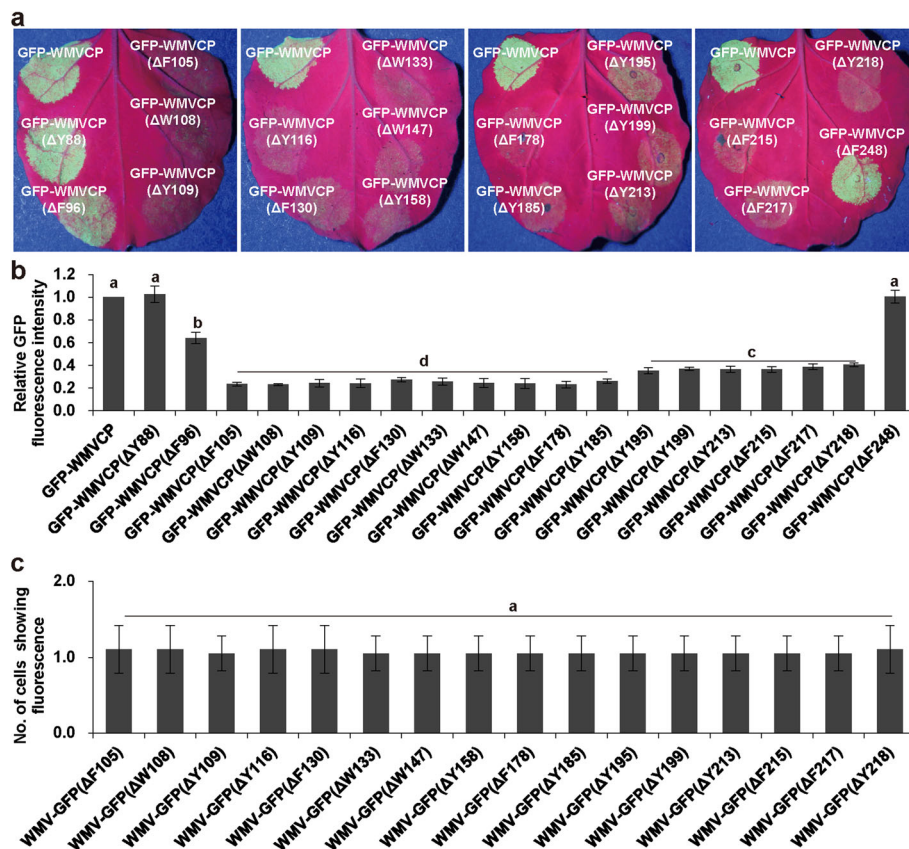


Fig. 7 Effects of π -stackings on CP accumulation and cell-to-cell movement of WMV. **a** GFP fluorescence and **b** relative GFP fluorescence intensities in the *N. benthamiana* leaf patches expressing GFP-WMVCP, one of its 16 mutants derived from aromatic residues (F¹⁰⁵, W¹⁰⁸, Y¹⁰⁹, Y¹¹⁶, F¹³⁰, W¹³³, W¹⁴⁷, Y¹⁵⁸, F¹⁷⁸, Y¹⁸⁵, Y¹⁹⁵, Y¹⁹⁹, Y²¹³, F²¹⁵, F²¹⁷ and Y²¹⁸) that could form π -stacking, or one of three mutants derived from aromatic residues (Y⁸⁸, F⁹⁶ and F²⁴⁸) that could not form π -stacking at 5 dpai. Pictures were photographed under UV light. GFP fluorescence intensity was determined by a multi-function microplate reader. **c** The number of cells showing GFP fluorescence per infection locus induced by 16 WMV-GFP mutants derived from aromatic residues (F¹⁰⁵, W¹⁰⁸, Y¹⁰⁹, Y¹¹⁶, F¹³⁰, W¹³³, W¹⁴⁷, Y¹⁵⁸, F¹⁷⁸, Y¹⁸⁵, Y¹⁹⁵, Y¹⁹⁹, Y²¹³, F²¹⁵, F²¹⁷ and Y²¹⁸) that could form π -stacking at 5 dpai. The values are the means \pm SD from 30 infection foci per treatment. Treatments marked with the same lowercase letters have no significant statistical difference. The inoculation tests were repeated three times independently. 'Δ' indicates the codon for the residue has been deleted

These results indicate that π -stackings play critical roles in maintaining the CP accumulation and cell-to-cell movement of WMV.

Discussion

Previous studies have shown that π -stacking formed by aromatic residues is involved in maintaining protein stability via stabilizing α -helices and β -sheets (Butterfield et al. 2002; Budyak et al. 2013). Recently, we have found that the aromatic rings of W¹²² (residue numbered according to the full length of TVBMV CP) in CPs of several potyvirus are critical for CP stability (Yan et al. 2021a). However, the mechanism of the ring of W¹²² in maintaining CP stability is unclear. In this study, we found that all 19 aromatic residues are located at the core region of TVBMV CP. Our prediction results showed that W¹²² and other 15 aromatic residues in the core regions of both TVBMV and WMV CPs could form π -stackings (Figs. 1 and 6; Additional file 1: Tables S1 and S2). Deletion of the aromatic residues that could form π -stackings significantly reduced CP accumulation to 20% of that of wild-type TVBMV CP. Furthermore, we found that substitutions of Y¹⁰⁵ and Y¹⁴⁷ individually with non-aromatic residues A or G significantly reduced TVBMV CP accumulation, while substitutions of Y¹⁰⁵ and Y¹⁴⁷ with aromatic residues F or W had little effect on TVBMV CP accumulation (Fig. 4a, b). Deletion of the aromatic residues that could form π -stackings also significantly reduced CP accumulation of WMV (Fig. 7a, b). These results imply that disturbing π -stacking in potyvirus CPs reduce the stability of the proteins, as a consequence, reduce their accumulation. We also found that the accumulation of GFP-TVBMVCP(Y105W) was lower than that of GFP-TVBMVCP(Y105F). The similar phenotype has been reported previously, which showed that a specific edge-to-face conformation between the Y⁵¹-F⁶⁴ pair of interacting aromatics is important for the fold and stability of SUMO, and substitution of Y⁵¹ with F⁵¹ could perturb the edge-to-face conformation and reduce SUMO stability (Chatterjee et al. 2019). It is also possible that Y⁵¹F substitution can create major distortions in the network of interactions between the pair and other residues at the buried environment of SUMO1 and then reduce protein stability (Chatterjee et al. 2019).

Our previous study has shown that mutation of W¹²² to non-aromatic residues remarkably reduces CP accumulation, virus replication and abolishes intercellular movement of TVBMV (Yan et al. 2021a). In consistent with these results, we further found that deletion mutation of any of the 16 aromatic residues, including W¹²² that could form π -stacking within CP, abolished TVBMV and WMV cell-to-cell movement (Figs. 3c and 7c). These mutations also significantly reduced CP accumulation and TVBMV replication (Figs. 2 and 3e). As efficient replication is the

prerequisite step for potyviral cell-to-cell movement (Deng et al. 2015; Chai et al. 2020), the low accumulation of CP and viral RNA might be responsible for the abolishment of cell-to-cell movement of TVBMV mutants.

Previous study has shown that TEV mutants derived from S¹²², R¹⁵⁴ and D¹⁹⁸ fail to move between cells and to form virus particles to a detectable level. Similar results are obtained in the corresponding point mutants of TuMV and WSMV (Tatineni et al. 2014; Dai et al. 2020). We have found that movement-defective TVBMV mutants derived from W¹²² form fewer virus particles compared with wild-type TVBMV (Yan et al. 2021a). Here, we also found that movement-defective TVBMV mutants, including TVBMV-GFP(Y105A), TVBMV-GFP(Y105G), TVBMV-GFP(Y147A) and TVBMV-GFP(Y147G), produced fewer virus particles compared with wild-type TVBMV-GFP and the movement-competent mutants including TVBMV-GFP(Y105F), TVBMV-GFP(Y105W), TVBMV-GFP(Y147F) and TVBMV-GFP(Y147W) (Fig. 5). Combined with the results in Additional file 2: Figure S1, it was showed that disrupting π -stackings formed by those aromatic amino acid residues reduced the accumulation level of CP (Additional file 2: Figure S1) and subsequently the number of virus particles. CP is an essential viral protein for cell-to-cell movement of potyviruses, which is transported through plasmodesmata in the form of virus particles or vRNA/CP interaction complex (Wang 2021). Our results suggest that π -stackings formed by those aromatic amino acid residues are important for the accumulation level of CP, and this can further affect virus movement.

Aromatic residues are usually essential for maintaining both protein structure and function. An aromatic residue in the readthrough protein may regulate systemic infection of potato leafroll virus together with an α -helix structural motif (Xu et al. 2018). Mutations of aromatic residues buried at the core of SUMO affect its conformation and therefore reduce interface affinity with SUMO interacting motifs of promyelocytic leukemia protein (Chatterjee et al. 2019). There is a possibility that mutations of aromatic residues affect CP conformation and impair interactions of CP with viral/host proteins.

The conserved residues are discontinuously distributed in the primary sequence and have a relationship in the 3D structure, which is critical for specific function of proteins. The conserved residues S¹⁴⁰, R¹⁷² and D²¹⁶ are located in the RNA-binding pocket of CP of WMV, PVY and TuMV, respectively (Zamora et al. 2017; Cuesta et al. 2019; Kežar et al. 2019, 2020). Residues R¹⁹² and K²²⁵ in RNA-binding pocket of TVBMV CP control virus cell-to-cell movement and replication (Yan et al. 2021b). Our results presented here further reveal the role of discontinuous conserved aromatic residues in the potyvirus CP

core region in forming π -stacking and maintaining CP stability and virus movement.

Conclusions

In this paper, we showed that the conserved aromatic residues in the core regions of TVBMV and WMV CPs were predicted to form π -stackings, which are critical for CP accumulation, potyvirus replication and viral cell-to-cell movement. These results support the conclusion that multiple evolutionarily conserved aromatic residues of CP are involved in potyvirus movement by forming π -stackings to maintain CP accumulation. This research provides novel insight into the role of evolutionarily conserved aromatic residues of CP in potyvirus infection.

Methods

The three-dimensional modeling and π -stacking analysis

Three-dimensional (3D) models in this study were predicted using the I-TASSER software (Yang et al. 2014). The centroid distance between two aromatic rings was measured using the PyMOL Molecular Graphics System (<https://pymol.org>).

Plasmid construction

The infectious clones pCamTVBMV-GFP (GenBank accession no: JQ407082) and pCBWMV-GFP (MN910314) were constructed previously by our laboratory (Gao et al. 2012; Ji 2020). The CP-encoding sequences of TVBMV and WMV were PCR-amplified from the above clones and individually ligated into the pCam35S::GFP vector to generate pCamGFP-TVBMVCP and pCamGFP-WMVCP to express different GFP-CP fusion proteins in *N. benthamiana* leaves. The mutant plasmids of pCamTVBMV-GFP, pCamWMV-GFP, pCamGFP-TVBMVCP and pCamGFP-WMVCP were produced using a site-directed mutagenesis technology as described previously (Liu and Naismith 2008). Primers used in this study were listed in Additional file 1: Table S3.

Plant growth and vector inoculation

N. benthamiana plants were grown in a greenhouse under controlled conditions (25 °C, 16/8 h light/dark photoperiod). Agrobacterium carrying infectious clone was cultured and diluted to an OD₆₀₀ of 0.2 for viral infectivity assay, and 0.0001 for viral cell-to-cell movement assay. For transient protein expression assay, agrobacterium (OD₆₀₀ = 0.4) carrying one of the expressing vectors was mixed at a ratio of 1:1 with agrobacterium (OD₆₀₀ = 0.4) carrying the pBinP19 vector expressing the RNA silencing suppressor P19 of tomato bushy stunt virus. The mixed agrobacterial cultures were infiltrated into leaves of 4–6 weeks old *N. benthamiana* plants. The inoculation tests were repeated three times independently.

Confocal microscopy and GFP imaging

To examine virus cell-to-cell movement, agroinfiltrated *N. benthamiana* leaves were harvested at 5 dpai and examined under a confocal microscope (Leica, Wetzlar, Germany) for viral cell-to-cell movement. The excitation wavelength was set at 488 nm and the emission wavelength was set at 520–540 nm. To record GFP fluorescence loci in the agroinfiltrated leaves, the leaves were photographed at 5 dpai using a digital camera (Canon 80D, Tokyo, Japan) under a hand-held UV lamp (LUYOR, Shanghai, China).

Measurement of GFP fluorescence intensity

Leaf discs of 5 mm in diameter were cut from agroinfiltrated leaves with a cork borer and individually placed in wells of 96-well microtiter plates. The intensity of GFP fluorescence for each disc was measured using a multi-function microplate reader (BioTek, Synergy™ Mx, Winoski, VT, USA) set at the 485/10 nm excitation wavelength and the 535/10 nm emission wavelength.

Western blotting

Western blotting assay was performed as described previously (Yan et al. 2021a). Total protein was extracted from *N. benthamiana* leaf tissues with extraction buffer (100 mM Tris-HCl, 150 mM NaCl, 1 mM EDTA, 5% sucrose and 1 mM phenylmethanesulfonyl fluoride). TVBMV CP antibody and horseradish peroxidase-conjugated goat anti-rabbit IgG (Sigma-Aldrich, St. Louis, MO, USA) were used as the primary and the secondary antibodies, respectively. After the addition of the SuperSignal™ West Dura Extended Duration Substrate solution (Thermo Fisher Scientific), the detection signal was visualized using a Chemiluminescent Imaging and Analysis System (Sage, Beijing, China).

ELISA

Tissues of 0.2 g in weight were collected from systemic leaves of the assayed *N. benthamiana* plants and individually homogenized in 400 μ L coating buffer (15 mM Na₂CO₃ and 35 mM NaHCO₃, pH 9.6). One hundred microliters of crude leaf extract were loaded into one well of a 96-well microtiter plate, with three wells used for each sample. The plate was incubated overnight at 4 °C. After four rinses with PBST buffer (80 mM Na₂HPO₄, 1.5 M NaCl, 20 mM KH₂PO₄, 30 mM KCl and 0.5% Tween-20 in distilled water, pH 7.4), an antibody solution specific for TVBMV CP was loaded into the wells followed by 4 h incubation at 37 °C. After four rinses with PBST buffer, an alkaline phosphatase-conjugated goat anti-rabbit IgG solution was added to each well and the plate was incubated at 37 °C for 4 h. Detection signal was developed by the addition of 100 μ L p-Nitrophenyl phosphate substrate (Sigma-

Aldrich, St. Louis, MO, USA) solution into each well and the optical density at 405 nm (OD_{405}) of each well was read using a multi-function microplate reader.

RNA isolation and RT-qPCR

Systemic leaf tissues (0.2 g per sample) were collected from leaves of the assayed *N. benthamiana* plants and used for total RNA isolation using TransZol reagent (TransGen Biotech, Beijing, China). Genomic DNA was removed from samples using a gDNA removal enzyme as instructed (Vazyme, Nanjing, China). Reverse transcription was performed in a reaction volume of 10 μ L containing 500 ng total RNA, 0.5 μ L HiScript II reverse transcriptase (200 U/ μ L, Vazyme), 0.5 μ L random primer (50 ng/ μ L) for detecting viral accumulation in system leaves, or 0.5 μ L specific primers qTVBMVCP-F (10 μ M) and EF1A-R (10 μ M) for detecting TVBMV (-)RNA accumulation. For RT-qPCR, 0.3 μ L cDNA was used in each 20 μ L reaction with virus-specific primers and a ChamQ SYBR qPCR master mix (Vazyme) on an LC96 qPCR system (Roche, Basel, Switzerland). In this study, the expression level of the *NbEF1A* gene was used as an internal control. The primers used in this study were listed in Additional file 1: Table S3. The RT-qPCR was performed with three biological replicates.

Virus particle purification

Six grams of infiltrated leaves were ground in liquid nitrogen and then homogenized in 12 mL extract buffer (0.2 M phosphate buffer, 0.15% β -mercaptoethanol and 0.01 M EDTA, pH = 8). The homogenate was centrifuged at 11,000 \times g for 20 min and then filtered through four layers of Miracloth (Millipore, Billerica, MA, USA). The supernatant was loaded on a 20% sucrose cushion at a ratio of 2:5 (vol/vol) and centrifuged for 1 h at 100,000 \times g, 4 $^{\circ}$ C (CP100WX, Hitachi, Tokyo, Japan). The pellets were resuspended overnight in 100 μ L of 0.02 M phosphate buffer (pH = 8) at 4 $^{\circ}$ C. The undissolved parts were removed by centrifugation at 8000 \times g for 20 min at 4 $^{\circ}$ C. The supernatant was loaded onto 230-mesh carbon-coated copper grids, washed with 2 drops of 0.02 M phosphate buffer (pH = 8), negatively stained with 2% phosphotungstic acid (PTA) (pH = 7), and then observed under a transmission electron microscope (JEM-1200Ex, Joel, Tokyo, Japan).

Statistical analyses

Statistical differences ($P < 0.05$) between the treatments were determined using Duncan's multiple range test in the SPSS (version 19) statistical software.

Abbreviations

CP: Coat protein; ELISA: Enzyme-linked immunosorbent assay; PVY: Potato virus Y; RT-qPCR: Reverse transcription-quantitative polymerase chain reaction; SMV: Soybean mosaic virus; SUMO: Small ubiquitin-like modifier;

TEV: Tobacco etch virus; TuMV: Turnip mosaic virus; TVBMV: Tobacco vein banding mosaic virus; WMV: Watermelon mosaic virus; ZYMV: Zucchini yellow mosaic virus

Supplementary Information

The online version contains supplementary material available at <https://doi.org/10.1186/s42483-021-00088-9>.

Additional file 1: Table S1. Centroid distances between rings of aromatic residues in TVBMV CP. **Table S2.** Centroid distances between rings of aromatic residues in WMV CP. **Table S3.** Primers used in this study.

Additional file 2: Figure S1. CP accumulation in the *N. benthamiana* leaf patches expressing TVBMVCP, TVBMV(Y105A), TVBMV(Y105G), TVBMV(Y147A) or TVBMV(Y147G) at 5 dpai. Ponceau red-stained nitrocellulose membrane-bound RuBisCO large subunit protein (Rubi) was used to show sample loadings. **Figure S2.** Alignment of 234 full-length CP sequences representing 127 potyviruses. The color scheme of residues shows different hydrophobicity. Blue indicates hydrophilic residues, green indicates neutral residues and black indicates hydrophobic residues. Positions of aromatic residues predicted to form π -stacking in TVBMV CP are indicated by arrowheads. The positions labeled with red and blue arrowheads indicate the completely and incompletely conserved residues for aromatic residues, respectively. **Figure S3.** Comparison of the predicted 3D model of TVBMV, WMV, PVY and TuMV CPs. Protein Data Bank (PDB) code: 6HXX for PVY CP, 5ODV for WMV CP and 6T34 for TuMV CP. The 3D model of TVBMV CP was predicted using the I-TASSER server. **Figure S4.** Alignment of TVBMV and WMV CP aromatic residues forming π -stackings.

Acknowledgments

We are grateful to Dr. Ping Qian from the College of Chemistry and Material Science, Shandong Agricultural University, China, and Dr. Hong Guo from the University of Tennessee, USA, for their valuable suggestions and discussions.

Authors' contributions

ZYY, YPT and XDL conceived the study; ZYY performed the experiments; CG contributed materials; ZYY, XJX and LF analyzed the data; ZYY wrote the paper with the collaboration of YPT and XDL. All authors read and approved the final manuscript.

Funding

This study was supported by grants from the National Natural Science Foundation of China (NSFC; 31720103912, 31871933), 'Taishan Scholar' Construction Project (TS201712023) and Funds of Shandong 'Double Tops' Program (SYL2017XTTD11).

Availability of data and materials

Not applicable.

Declarations

Ethics approval and consent to participate

Not applicable.

Consent for publication

Not applicable.

Competing interests

The authors declare that they have no competing interests.

Author details

¹Laboratory of Plant Virology, College of Plant Protection, Shandong Agricultural University, Tai'an, Shandong 271018, People's Republic of China. ²Shandong Provincial Key Laboratory of Agricultural Microbiology, Shandong Agricultural University, Tai'an, Shandong 271018, People's Republic of China.

Received: 10 December 2020 Accepted: 30 April 2021
Published online: 21 May 2021

References

- Budyak IL, Zhuravleva A, Gierasch LM. The role of aromatic-aromatic interactions in strand-strand stabilization of β -sheets. *J Mol Biol.* 2013;425(18):3522–35. <https://doi.org/10.1016/j.jmb.2013.06.030>.
- Burley SK, Petsko GA. Aromatic-aromatic interaction: a mechanism of protein structure stabilization. *Science.* 1985;229(4708):23–8. <https://doi.org/10.1126/science.3892686>.
- Butterfield SM, Patel PR, Waters ML. Contribution of aromatic interactions to α -helix stability. *J Am Chem Soc.* 2002;124(33):9751–5. <https://doi.org/10.1021/ja026668q>.
- Chai M, Wu X, Liu J, Fang Y, Luan Y, Cui X, et al. P3N-PIPO interacts with P3 via the shared N-terminal domain to recruit viral replication vesicles for cell-to-cell movement. *J Virol.* 2020;94:e01898–19.
- Chatterjee KS, Tripathi V, Das R. A conserved and buried edge-to-face aromatic interaction in small ubiquitin-like modifier (SUMO) has a role in SUMO stability and function. *J Biol Chem.* 2019;294(17):6772–84. <https://doi.org/10.1074/jbc.RA118.006642>.
- Cuesta R, Yuste-Calvo C, Gil-Cartón D, Sánchez F, Ponz F, Valle M. Structure of turnip mosaic virus and its viral-like particles. *Sci Rep.* 2019;9(1):15396. <https://doi.org/10.1038/s41598-019-51823-4>.
- Dai Z, He R, Bernards MA, Wang A. The cis-expression of the coat protein of turnip mosaic virus is essential for viral intercellular movement in plants. *Mol Plant Pathol.* 2020;21(9):1194–211. <https://doi.org/10.1111/mpp.12973>.
- Deng P, Wu Z, Wang A. The multifunctional protein CI of potyviruses plays interlinked and distinct roles in viral genome replication and intercellular movement. *Virology.* 2015;12(1):141. <https://doi.org/10.1186/s12985-015-0369-2>.
- Dolja W, Haldeman R, Robertson NL, Dougherty WG, Carrington JC. Distinct functions of capsid protein in assembly and movement of tobacco etch potyvirus in plants. *EMBO J.* 1994;13(6):1482–91. <https://doi.org/10.1002/j.1460-2075.1994.tb06403.x>.
- Dolja W, Haldeman-Cahill R, Montgomery AE, Vandenbosch KA, Carrington JC. Capsid protein determinants involved in cell-to-cell and long distance movement of tobacco etch potyvirus. *Virology.* 1995;206(2):1007–16. <https://doi.org/10.1006/viro.1995.1023>.
- Gao R, Tian Y-P, Wang J, Yin X, Li X-D, Valkonen JPT. Construction of an infectious cDNA clone and gene expression vector of tobacco vein banding mosaic virus (genus *Potyvirus*). *Virus Res.* 2012;169(1):276–81. <https://doi.org/10.1016/j.virusres.2012.07.010>.
- Geng C, Yan Z-Y, Cheng D-J, Liu J, Tian Y-P, Zhu C-X, et al. Tobacco vein banding mosaic virus 6K2 protein hijacks NbPsbO1 for virus replication. *Sci Rep.* 2017; 7(1):43455. <https://doi.org/10.1038/srep43455>.
- Hillier BJ, Rodriguez HM, Gregoret LM. Coupling protein stability and protein function in *Escherichia coli* CspA. *Fold Des.* 1998;3(2):87–93. [https://doi.org/10.1016/S1359-0278\(98\)00014-5](https://doi.org/10.1016/S1359-0278(98)00014-5).
- Hong H, Park S, Jiménez RHF, Rinehart D, Tamm LK. Role of aromatic side chains in the folding and thermodynamic stability of integral membrane proteins. *J Am Chem Soc.* 2007;129(26):8320–7. <https://doi.org/10.1021/ja068849o>.
- Huang CH, Hsiao WR, Huang CW, Chen KC, Lin SS, Chen TC, et al. Two novel motifs of watermelon silver mottle virus NSs protein are responsible for RNA silencing suppression and pathogenicity. *PLoS One.* 2015;10(5):e0126161. <https://doi.org/10.1371/journal.pone.0126161>.
- Ji S. Study on genetic diversity and long-distance movement determinants of watermelon mosaic virus. M. Sc. thesis, Shandong Agricultural University. 2020.
- Kežar A, Kavčič L, Poláčik M, Nováček J, Gutiérrez-Aguirre I, Žnidarič MT, et al. Structural basis for the multitasking nature of the potato virus Y coat protein. *Sci Adv.* 2019;5:eaaw3808.
- Kimalov B, Gal-On A, Stav R, Belausov E, Arazi T. Maintenance of coat protein N-terminal net charge and not primary sequence is essential for zucchini yellow mosaic virus systemic infectivity. *J Gen Virol.* 2004;85(Pt 11):3421–30. <https://doi.org/10.1099/vir.0.80417-0>.
- Liu H, Naismith JH. An efficient one-step site-directed deletion, insertion, single and multiple-site plasmid mutagenesis protocol. *BMC Biotechnol.* 2008;8(1): 91. <https://doi.org/10.1186/1472-6750-8-91>.
- Marcotrigiano J, Gingras AC, Sonenberg N, Burley SK. Cocystal structure of the messenger RNA 5' cap-binding protein (eIF4E) bound to 7-methyl-GDP. *Cell.* 1997;89(6):951–61. [https://doi.org/10.1016/S0092-8674\(00\)80280-9](https://doi.org/10.1016/S0092-8674(00)80280-9).
- Matsuo H, Li H, McGuire AM, Fletcher CM, Gingras AC, Sonenberg N, et al. Structure of translation factor eIF4E bound to m⁷GDP and interaction with 4E-binding protein. *Nat Struct Mol Biol.* 1997;4(9):717–24. <https://doi.org/10.1038/nsb0997-717>.
- Salonen LM, Ellermann M, Diederich F. Aromatic rings in chemical and biological recognition: energetics and structures. *Angew Chem Int Ed.* 2011;50(21): 4808–42. <https://doi.org/10.1002/anie.201100756>.
- Seo JK, Vo Phan MS, Kang SH, Choi HS, Kim KH. The charged residues in the surface-exposed C-terminus of the soybean mosaic virus coat protein are critical for cell-to-cell movement. *Virology.* 2013;446(1-2):95–101. <https://doi.org/10.1016/j.virol.2013.07.033>.
- Serrano L, Bycroft M, Fersht AR. Aromatic-aromatic interactions and protein stability. *J Mol Biol.* 1991;218:465–75.
- Shukla DD, Strike PM, Tracy SL, Gough KH, Ward CW. The N and C termini of the coat proteins of potyviruses are surface-located and the N terminus contains the major virus-specific epitopes. *J Gen Virol.* 1988;69(7):1497–508. <https://doi.org/10.1099/0022-1317-69-7-1497>.
- Tatinen S, Kovacs F, French R. Wheat streak mosaic virus infects systemically despite extensive coat protein deletions: identification of virion assembly and cell-to-cell movement determinants. *J Virol.* 2014;88(2):1366–80. <https://doi.org/10.1128/JVI.02737-13>.
- Wang A. Cell-to-cell movement of plant viruses via plasmodesmata: a current perspective on potyviruses. *Curr Opin Virol.* 2021;48:10–6. <https://doi.org/10.1016/j.coviro.2021.03.002>.
- Weber PH, Bujarski JJ. Multiple functions of capsid proteins in (+) stranded RNA viruses during plant-virus interactions. *Virus Res.* 2015;196:140–9. <https://doi.org/10.1016/j.virusres.2014.11.014>.
- Xu Y, Da Silva WL, Qian Y, Gray SM. An aromatic amino acid and associated helix in the C-terminus of the potato leafroll virus minor capsid protein regulate systemic infection and symptom expression. *PLoS Pathog.* 2018;14:e1007451.
- Yan Z-Y, Cheng D-J, Liu L-Z, Geng C, Tian Y-P, Li X-D, et al. The conserved aromatic residue W¹²² is a determinant of potyviral coat protein stability, replication, and cell-to-cell movement in plants. *Mol Plant Pathol.* 2021a; 22(2):189–203. <https://doi.org/10.1111/mpp.13017>.
- Yan Z-Y, Xu X-J, Fang L, Cheng D-J, Tian Y-P, Geng C, et al. Residues R¹⁹² and K²²⁵ in RNA-binding pocket of tobacco vein banding mosaic virus CP control virus cell-to-cell movement and replication. *Mol Plant-Microbe Interact.* 2021b. <https://doi.org/10.1094/MPMI-09-20-0265-R>.
- Yang J, Yan R, Roy A, Xu D, Poisson J, Zhang Y. The I-TASSER suite: protein structure and function prediction. *Nat Methods.* 2014;12:7–8.
- Zamora M, Méndez-López E, Aguirrezabala X, Cuesta R, Lavín JL, Sánchez-Pina MA, et al. Potyvirus virion structure shows conserved protein fold and RNA binding site in ssRNA viruses. *Sci Adv.* 2017;3:eaa02182.

Ready to submit your research? Choose BMC and benefit from:

- fast, convenient online submission
- thorough peer review by experienced researchers in your field
- rapid publication on acceptance
- support for research data, including large and complex data types
- gold Open Access which fosters wider collaboration and increased citations
- maximum visibility for your research: over 100M website views per year

At BMC, research is always in progress.

Learn more [biomedcentral.com/submissions](https://www.biomedcentral.com/submissions)

